Original Research Report

Dkk2 ***interacts with*** **Pax9** ***in palate mesenchyme to pattern and tune osteogenesis***

Jeremie Oliver Piña[1,2], Daniela M. Roth[1,3], Resmi Raju[1], Emma Wentworth Winchester[4], Parna Chattaraj[1], Fahad Kidwai[1], Fabio R. Faucz[5], James Iben[5], Cameron Padilla[5], Justin L. Cotney[6], Rena N. D'Souza[1*]

RUNNING TITLE: ***Wnt genes pattern palatal bone***

[1]Section on Craniofacial Genetic Disorders**,** *Eunice Kennedy Shriver* National Institute of Child Health and Human Development, National Institutes of Health, Bethesda, MD, USA.

[2]Department of Biomedical Engineering, University of Utah, Salt Lake City, UT, USA.

[3]School of Dentistry, University of Alberta, Edmonton, AB, CA.

[4]University of Connecticut School of Dental Medicine, Farmington, CT, USA.

[5]Molecular Genomics Core*, Eunice Kennedy Shriver* National Institute of Child Health and Human Development, National Institutes of Health, Bethesda, MD, USA.

[6]Department of Genetics and Genome Sciences, University of Connecticut School of Medicine, Farmington, CT, USA.

**Corresponding author*: Rena N. D'Souza, D.D.S., M.S., Ph.D.
Director, National Institute of Dental and Craniofacial Research
Chief, Section on Craniofacial Genetic Disorders
Eunice Kennedy Shriver National Institute of Child Health and Human Development
9000 Rockville Pike, Bethesda, MD, USA 20892
Tel: (713) 398-9100; Email: Rena.D'Souza@nih.gov

KEYWORDS: Palatogenesis; Osteogenesis; Wnt signaling; Patterning; Multiomics; Spatial biology

SUMMARY STATEMENT

Novel evidence of Wnt-mediated osteogenic differentiation and patterning of palatal bone is presented in a murine cleft palate model. *Dkk2* is implicated as a spatial regulator of palate ossification zones, in concert with *Pax9*.

ABSTRACT

Cleft palate is a common craniofacial disorder involving multiple genetic and environmental predisposing factors. Currently, limited insight exists into the molecular mechanisms regulating osteogenic differentiation and patterning in the palate during embryogenesis. This study utilized the *Pax9*-deficient mouse genetic model of cleft palate to investigate the role of *Pax9* in osteogenic differentiation. Single-nucleus transcriptomics and chromatin accessibility assays validated by whole-transcriptome and single-molecule spatial transcriptomics suggest a relationship between separate *Pax9*+ and osteogenic populations. Loss of *Pax9* resulted in premature osteogenic differentiation and bone maturation. The spatially restricted osteogenic domains in *Pax9*$^{-/-}$ mice are bounded by *Dkk2*, which normally interfaces with *Pax9* in the mesenchyme. Together, these results confirm a regulatory role for the Wnt pathway in patterning of palatal bone, offering novel insights into the complex nature of developmental signaling and osteodifferentiation in the palate.

50 **INTRODUCTION**

51 Palatal morphogenesis involves a complex interplay of cell adhesion molecules, epigenetic
52 regulators, transcription factors, and overlapping signaling pathways (Ji et al., 2020, Reynolds et
53 al., 2019). It is well known that spatiotemporal molecular cues drive region-specific growth,
54 migration, elevation, and midline fusion of the palatal shelves (Bush and Jiang, 2012, Li et al.,
55 2017a). As for other intramembranous models, palatal osteogenesis first becomes evident as a
56 focal area of mesenchymal condensation that subsequently functions as an ossification center
57 (Wang et al., 2020, Baek et al., 2011, Li et al., 2021). While our recent work has highlighted the
58 spatiotemporal transcriptional programming requisite for normal palatal osteogenesis to occur
59 (Piña et al., 2023), the precise molecular mechanisms that modulate the differentiation and
60 spatial patterning of palatal osteoblasts during morphogenesis are not well defined (Oliver et al.,
61 2021). Such knowledge will improve our understanding of these mechanistic underpinnings to
62 better advance the development of novel therapeutic interventions for patients affected with cleft
63 disorders (Oliver et al., 2020).

64

65 The Wnt/β-catenin signaling pathway has an important regulatory role in the development and
66 homeostasis of the skeleton (Huybrechts et al., 2020, Joeng et al., 2017, Krishnan et al., 2006)
67 and is known to be essential for craniofacial development. We and others have shown that Wnt
68 signaling pathway genes play crucial roles in early palate formation, specifically driving
69 mesenchymal cell proliferation and differentiation (Jia et al., 2020, Jia et al., 2017a, Li et al.,
70 2017b, Jia et al., 2017b, Janeckova et al., 2023). Intracellular mediators of canonical Wnt
71 signaling, such as beta-catenin, promote lineage specification of mesenchymal stem cells and the
72 differentiation of osteogenic precursors into functional osteoblasts and osteocytes (Cruciat and

Niehrs, 2013, Glass et al., 2005, Kim et al., 2013). Notably, mutations in coding sequences of Wnt factors result in skeletal dysplasias with clinical phenotypes that involve isolated alterations in bone mass (Martinez-Gil et al., 2022, Regard et al., 2011).

The paired homeodomain-containing transcription factor, Pax9, serves critical functions in mammalian development and organogenesis including the patterning of limbs and craniofacial structures (Peters et al., 1998, Peters et al., 1999). *PAX9* has been identified as crucial for human craniofacial development through genome-wide association studies (GWAS), which implicated it in several disorders affecting the face, such as non-syndromic clefting (Shaffer et al., 2016). Furthermore, the temporally dynamic antero-posterior morphogenetic gradient of *Pax9* in the palate indicates its central role in palatogenesis (Jia et al., 2020, Hilliard et al., 2005). *Pax9* knockout mice demonstrate defects in elongation, delayed elevation, and failed contact and fusion of the palatal shelves (Jia et al., 2017a, Peters et al., 1998). The regulatory role of *Pax9* in orchestrating overlapping pathways such as Shh, Eda, Fgf, and Wnt signaling has previously been established and is appreciated in the context of secondary palate development (Ji et al., 2020, Reynolds et al., 2019). Nevertheless, the exact role of *Pax9* in osteogenesis in the secondary palate remains speculative.

Here, we demonstrate that global loss of *Pax9* results in altered spatiotemporal patterning and consequent premature differentiation of the osteogenic condensation. By dissecting the spatial transcriptomic milieu of osteogenic commitment and terminal differentiation in the cleft palate of *Pax9* knockout mouse embryos, we present a Wnt-centered framework for osteogenic patterning, the balance of which depends on the regulatory influence of *Pax9.* This study expands

96 contemporary understanding of the functional roles played by *Pax9* and its overlapping Wnt
97 modulators to palate osteogenic patterning and differentiation.
98
99 **RESULTS AND DISCUSSION**
100 **The spatiotemporal expression domain of *Pax9* guides, but is not required for, subsequent**
101 **osteogenic differentiation in the developing palate.**
102 We began this study by contextualizing *Pax9* within normal palate osteogenesis in mice using
103 spatially resolved, quantitative whole-transcriptome RNA-sequencing (Visium, 10x Genomics,
104 Inc.). At embryonic day 13.5 (E13.5), the palatal shelves had not yet elevated, and ossification
105 was not evident, though the initial mesenchymal condensation that would give rise to bone could
106 be detected (**Fig. 1A**). *Pax9* was most highly expressed at bordering edges of *Sp7+* regions,
107 bounding more mature osteoblast *Cd200* expression (**Fig. 1B**). The palate mesenchyme had
108 fused by E15.5 and mineralizing bone was evident histologically with condensations of cells
109 arranged at medial, lateral, and superior edges of the palatine ossification center (**Fig. 1A**).
110 Interestingly, *Pax9* expression was maximally enriched within the medial palate mesenchyme, a
111 region which is also enriched for progenitor cell markers (*Six2, Erg, Crabp1*) (**Fig. 1B, B'**). This
112 expression was mirrored in adjacent lateral compartments by markers of osteoblast commitment
113 (*Sp7*, *Cd200*, **Fig. 1B, B'**), with highest enrichment surrounding the ossification centers and
114 radiating outward in a decreasing gradient of expression. The osteogenic compartment, with
115 comparatively lower *Pax9* expression than mesenchymal, is enriched for osteoblast (*Cd200,*
116 *Bglap, Ifitm5)* and osteocyte (*Sost, Dmp1, Phex*) markers. This expression gradient and inverse
117 osteogenic/mesenchymal enrichment suggested that *Pax9* was linked to the gradual formation of

118 bone during embryonic palate development, perhaps guiding the eventual patterning of
119 osteogenesis (Paudel et al., 2022).
120
121 We followed this observation with assessment of cell type-specific *Pax9* expression and binding
122 motif enrichment via integrated single-nucleus gene (snRNA)- and transposase-accessible
123 chromatin (snATAC)-sequencing of microdissected secondary palate tissues from E13.5 and
124 E15.5 mouse embryos. Initial clustering of this dataset revealed ten distinct cell states (**Fig. S1**).
125 Gene ontology enrichment analysis of marker genes from these populations determined the
126 presence of six general cell types: epithelium, mesenchyme, muscle cells, neural cells,
127 endothelium, and blood cells (**Fig. C'**, **Fig. S1**). Further isolated analysis of the mesenchyme
128 identified eight subtypes of this population. Canonical marker genes separate these cells into four
129 broad categories: osteogenic cells, chondrogenic cells, generalized mesenchyme, and *Pax9*+
130 mesenchyme (**Fig. S2**).
131
132 When compared to all cell types in the developing palate, we observed that the population of
133 *Pax9*+ mesenchymal cells demonstrated a 3.62 $\log_2$-fold enrichment of *Pax9* expression (FDR
134 3.01e-04) (**Fig. 1C"**). Similarly, we noted a bias of the *Pax9* motif within marker peaks for the
135 *Pax9* mesenchyme cluster, confirming enrichment of the *Pax9* motif within regions of accessible
136 chromatin unique to this population (marker peaks) (**Fig. 1C'''**). Notably, chromatin regions
137 accessible in the osteogenic cell population were depleted for the *Pax9* motif and demonstrated
138 minimal *Pax9* expression. Hence, while *Pax9* is important for a specific mesenchymal
139 population, it is not required for osteogenic cells.
140

141 **Ossification centers in *Pax9*$^{-/-}$ embryos differentiate and mature precociously.**

142 Next, we sought to understand the effects of global loss of *Pax9* on establishment of the
143 osteogenic condensation in the secondary palate, considering its mesenchymal expression
144 surrounding osteogenic compartments. At E13.5, when wild type bone formation in the palate
145 was minimal, *Pax9*$^{-/-}$ mice had a subtle increase in overall birefringent intensity of bundled
146 collagen, indicating a prematurely active osteogenic condensation (**Fig. 2A, A'**). By E15.5, the
147 amount of collagen was greater in corresponding regions of the palatal shelves in *Pax9*$^{-/-}$ embryos
148 (**Fig. 2B, B'**). The interface between cells lining the bone and the presumptive osteoid they
149 deposited was less fibrillar, with clearly defined bone edges (**Fig. B', C)**. Additionally, we noted
150 hallmark features of maturing bone in the *Pax9*$^{-/-}$ palate, such as greater trabeculation and
151 comparatively more *Sost*$^{+}$ mature osteocytes in the developing palatine bone when compared
152 with age-matched wild type embryos (**Fig. 2C**). Micro-computed tomography revealed three-
153 dimensional insufficiency of the mesial ossification front of this bone at E15.5, despite
154 indications of mature bone (**Fig. 2D'**). Coronal cross-sectional analysis exhibited dense, spongy
155 bone in knockout mice. These features of *Pax9*$^{-/-}$ palatal bone could indicate that, in the absence
156 of *Pax9*, bone undergoes accelerated mineralization and remodeling events which may restrict
157 the shelves' ability to achieve contact at the midline through sufficient inward growth.

158

159 **Osteogenic differentiation is spatially restricted and focally accelerated in *Pax9*$^{-/-}$ embryos.**

160 The early appearance of more mature bone in the absence of *Pax9* led us to assess the osteogenic
161 front of the secondary palate in this context. In normal development of the palate at E13.5, pre-
162 osteoblast *Runx2*$^{+}$ cells span the length of the mesial nasal domain of the palatal shelves,
163 expressed in both epithelium and mesenchyme (**Fig. 3A**). However, the domain of *Runx2* was

more restricted to the superior portion of the nasal domain in *Pax9*$^{-/-}$ embryos. *Six2* expression filled the *Runx2*- space of the palatal shelf in both *Pax9*$^{+/+}$ and *Pax9*$^{-/-}$ embryos, but the RNAscope *in situ* fluorescent signal appeared more granular in *Pax9*$^{-/-}$ cells. In wild type cells, *Six2* and *Runx2* subcellular expression was organized in a concentric pattern, with central *Runx2* nuclear expression. This distinctive transcript localization was absent in *Pax9* knockout cells, and the transition between *Six2+/Runx2-* to *Six2-/Runx2+* cells was less clear. We noted marked appearance of the maturing osteocyte marker *Dmp1* within the central ossification zone of *Pax9*$^{-/-}$ palatal shelves only, evidence of accelerated osteogenic differentiation.

By E15.5, an osteogenic gradient had been established in both wild type and *Pax9*$^{-/-}$ palatal shelves, emanating from the ossification center(s) (**Fig. 3B**). This differentiation gradient from *Runx2+* pre-osteoblasts to *Sp7+* osteoblasts to *Dmp1+* osteocytes terminated at the bone center (**Fig 3B'**). The osteogenic *Pax9*$^{-/-}$ front appeared proportionally compressed compared with wild type bone surfaces. However, the *Runx2+* region was extended, with disruption centrally by a zone of *Dkk2* positivity (**Fig. 3B"**). While *Dkk2* was found in the *Runx2+/Sp7+* region in isolated wild type cells, it occupied a broader region in the *Pax9*-deficient context, corresponding to regionally diminished *Runx2* expression.

A key phase in osteodifferentiation is the transition at bone front interfaces from *Runx2+* to *Dmp1+* cells. In wild type embryos, differentiating osteogenic populations were evenly and somewhat linearly spaced from *Runx2+/Sp7-* cells to *Runx2+/Sp7+/Dmp1-*, to more mature exclusively *Dmp1* expressing cells (**Fig. 3C', 3C''**). It was difficult to distinguish a clear progression of committed cell populations in the *Pax9*-null palate, with an abrupt transition

187 between *Runx2+/Sp7-* populations to *Runx2-/Sp7-/Dmp1+* cells. Very few cells expressed *Sp7* in
188 the absence of *Runx2* or *Dmp1*. Based on the disorganization of osteodifferentiation in the *Pax9*$^{-/-}$
189 palatine bone, we questioned whether *Pax9* may be responsible for commitment of cells to the
190 osteogenic lineage.
191
192 **Wnt modulators interact with *Pax9* to define spatiotemporal ossification domains in the**
193 **palate.**
194 The disruption of *Runx2* expression by *Dkk2* in *Pax9*$^{-/-}$ embryos called to mind prior evidence of
195 *Pax9* in patterning of palate mesenchyme, and how this relates to the regulatory role of the Wnt
196 signaling pathway in skeletal development and homeostasis (Nagasaka et al., 2022, Zhou et al.,
197 2013, Hamachi et al., 2003, Sasaki et al., 2007). Thus, we sought to interrogate the zones of
198 osteogenic patterning and differentiation in the secondary palate overlaying Wnt pathway
199 modulators known to interact with Pax9 directly (*Dkk1* and *Dkk2*). *Pax9* was strongly expressed
200 in the palatal shelf at E13.5, with predilection toward the oral domain of the vertically oriented
201 shelf prior to elevation above the tongue (**Fig. 4A)**. We observed that the pattern of *Alpl*
202 expression, corresponding to osteogenesis, was complemented by *Pax9* and Wnt modulators
203 *Dkk1* and *Dkk2*. *Dkk1* was expressed within the domain of *Pax9*, which was found in regions
204 inferior to *Alpl* expression, clearly interfacing midway through the medial side of the nasal
205 domain of the palate, corroborating our initial transcriptomic observations. *Dkk2* co-localized
206 with *Pax9* in the lateral oral domain. In the control palate, *Dkk2+* cells were also interspersed
207 amongst *Alpl+* cells in the nasal domain of the palate.
208

209 In the absence of *Pax9*, *Alpl* was focally increased in the superior aspect of the nasal domain,
210 with similar spatial restriction in the more lateral ossification center (**Fig. 4A**). *Dkk1* was lost in
211 regions where it is normally co-expressed with *Pax9* but increases at the point of maximal *Alpl*
212 expression. We hypothesized that this was due to the premature terminal differentiation of
213 osteocytes, which express *Dkk1* (Dincel et al., 2022). *Dkk2* positivity expanded downward into
214 the tip of the knockout palatal shelf into the space occupied by *Pax9* in the wild type palate,
215 overlapping with *Alpl*+ cells in the margins of the ossification center. However, *Dkk2* was absent
216 from the central region of this highly *Alpl*-enriched condensation (**Fig. 4B**). In the *Pax9*-
217 knockout setting, *Dkk2* expression encapsulated the ossification center, restricting the
218 *Dkk1+/Dkk2-/Alp1+* condensation (**Fig. 4C**).
219
220 Pax9 is a master orchestrator of patterning and morphogenesis throughout the body – from the
221 thymus, ultimobranchial bodies, limb bud, and tooth organ, to the axial skeleton (Peters et al.,
222 1998, Peters et al., 1999). This highly conserved morphogen has been shown to functionally
223 interact with a number of mesenchymal transcription factors and signaling pathways required for
224 palate development to ensue, which regulate cell proliferation and differentiation of cranial
225 neural crest-derived mesectoderm (Hilliard et al., 2005, Ichikawa et al., 2006, Jia et al., 2020, Jia
226 et al., 2017a, Li et al., 2017b, Neubuser et al., 1997). The role of Pax9 in patterning during
227 development of multiple organ systems, including the palate, are clearly established. However,
228 prior to the present study, this has not been explored sufficiently in the context of palate
229 osteogenesis. The resultant cleft palate phenotypes in the setting of either premature (Mori-
230 Akiyama et al., 2003, Sweat et al., 2020) or delayed (Baek et al., 2011) palate osteogenesis
231 exemplify the importance of precise temporal onset and spatial regulation of intramembranous

232 ossification. The unusually broad expression of *Six2* and precocious, restricted osteogenesis in
233 the *Pax9*$^{-/-}$ palate mesenchyme are reminiscent of the premature ossification and cleft palate
234 described in *Sox9*$^{-/-}$ (Mori-Akiyama et al., 2003) and *Six2*$^{-/-}$ mice (Sweat et al., 2020). Sweat *et al*.
235 further noted a direct up-stream regulatory relationship between the osteoprogenitor transcription
236 factor, Six2, and Pax9, supporting a predicted role for Pax9 in progression of palate osteogenesis,
237 and perhaps explaining the broad presence of *Six2*+ cells in the absence of *Pax9*. It should be
238 noted that initial formation of osteogenic centers and ability to form bone are not directly
239 affected by the *Pax9*$^{-/-}$ mutation. However, the spatial patterning and osteodifferentiation
240 mechanics in the palate appeared to be dysregulated in its absence.

241

242 In summary, this study addresses the perturbation of osteogenic patterning and differentiation in
243 relation to Wnt signaling mediators in the *Pax9*$^{-/-}$ genetic model of secondary cleft palate. We
244 characterized the onset of premature osteogenic differentiation as well as spatial restriction of
245 committed osteogenic cells in the absence of *Pax9*, pointing to its role in patterning and tuning
246 osteogenesis in the palate. This contribution to our fundamental understanding of the molecular
247 and cellular underpinnings of a cleft palate phenotype strengthens the framework required to
248 assess the safety and efficacy of targeted therapeutic strategies to prevent or correct cleft palate
249 disorders.

250

251

252

253

254 **MATERIALS AND METHODS**

255 *Animals.*

256 All animal procedures were approved by the National Institutes of Health, National Institute of
257 Child Health and Human Development Animal Care and Use Committee (ACUC), under Animal
258 Study Protocol (ASP) #21-031. C57BL/6J mice were obtained from the Jackson Laboratory.
259 Inbred strain of female C57BL/6 mice were utilized for all experiments. *Pax9*$^{+/-}$ mice were
260 provided by Dr. Rulang Jiang (Cincinnati Children's Hospital). Timed pregnancies were
261 conducted via vaginal plug identification, with day 0.5 indicating date of identification.

262 *Single-nucleus RNA + ATAC Sequencing* (*Multiome-RNA+ATAC-seq, 10x Genomics*).

263 Pregnant mice were sacrificed by CO_2 inhalation and cervical dislocation. All surgical
264 procedures were performed by using a surgical loupe (Orascoptic, Eye Zoom, 5.5x
265 magnification). Pregnant mice were placed in the supine position on a sterile, absorbent surgical
266 pad and disinfected with 70% ethanol along the site of planned incision. An incision was made
267 on the abdomen along the midline using small surgical scissors. A fresh microsurgical scissor
268 was then used to carefully incise the peritoneum to expose the uterine chain. Using a blunt
269 forceps, the uterine chain was externalized. Embryos were dissected out by releasing it along the
270 myometrium, incising at the oviduct bilaterally and the median uterine horn ligament attachment.
271 Whole embryos were transferred into ice-cold sterile PBS in a 10 cm petri dish. Each embryo
272 was carefully dissected out from the uterus and extra-embryonic amnion and chorionic tissues,
273 then transferred to a new 10 cm culture dish with fresh ice-cold PBS. A blunt forceps was used
274 to hold each embryo and by using a small fine microsurgical scissor, an incision was made on
275 bilateral oral commissures, allowing for extended opening of the mandible and clear vision of the

276 palate cranially. Careful microdissection of the palatal shelves only from respective embryonic
277 stages was performed, with noted potential extra-palatal tissue contamination due to surgical
278 imprecision. Pooled littermates (n=3 biological replicates per sample) of each respective stage
279 were utilized single nucleus dissociation (E13.5 and E15.5); 3 embryos' tissues per timepoint
280 were pooled into 1 sample per timepoint. Samples were mechanically broken into single-nuclei
281 suspensions following the manufacturer's instructions for Nuclei Isolation from Complex
282 Tissues for Single Cell Multiome ATAC + Gene Expression Sequencing (10X Genomics -
283 protocol CG000375). After isolation, the nuclei integrity was accessed under a microscope and
284 counted using the CellDrop (Denovix) and acridine orange (AO) and propidium iodide (PI) as
285 dye. Transposition and Gel Bead-in-Emulsion (GEM) generation, using a Chromium Single Cell
286 Multiome ATAC + 3′ Gene Expression following the manufacturer's instructions (10x Genomics
287 – protocol CG000338 Rev F) were performed, aiming for a total of 10,000 nuclei per sample. In
288 brief, the nuclei were transposed in a bulk solution using Tn5 transposase with sequencing
289 adapters that were pre-loaded. The transposed nuclei were loaded onto a microfluidic chip to
290 create GEMs. The gel beads contained two types of oligos that were used for snRNA-seq and
291 snATAC-seq. The mRNA was reverse transcribed and underwent template switching and
292 transcript extension to produce barcoded cDNA. The snATAC-seq oligo was formed of a partial
293 Illumina primer sequence, a 10X barcode, and a spacer that allowed the barcode to attach to the
294 adapter-tagged DNA fragments. The GEMs were broken using a recovery agent to produce a
295 bulk pool of barcoded molecules. The pre-amplified product was then split into portions
296 available for snRNA-seq and snATAC-seq library construction. P5, i7, and P7 sequences
297 compatible with Illumina bridge amplification were added to the DNA fragments through PCR
298 to produce snATAC-seq libraries. Additional amplification of the cDNA was performed on the

299 snRNA-seq samples before proceeding to fragmentation, end repair, A-tailing, and ligation. A
300 sample dual index PCR was used to add the P5, i5, i7, and P7 sequences to the final snRNA-seq
301 library. Sequencing was performed on the Illumina NovaSeq 6000 at the Molecular Genomics
302 Core (NICHD).

303 *Single-nucleus RNA + ATAC-seq bioinformatics analysis*.

304 Raw fastqs were aligned to mm10 genome build using the standard Cellranger multiomics
305 settings and imported to ArchR (v.1.0.1). Doublets were identified and filtered, and cells were
306 filtered for minimum 4 TSS enrichment, 2500 fragments per cell. Dimensionality reduction was
307 performed using LSI based on the cell by fragment matrix and cell by gene matrix, and clusters
308 were identified. Peaks were called based on original clustering, discarding reads from promoters
309 (2500bp +/- TSS) and exons. Cluster assignments were confirmed using canonical marker genes
310 based on gene expression, and gene ontology enrichment of marker genes identified using
311 getMarkerFeatures function of ArchR. Statistical significance and strength of enrichments was
312 determined using t-test, grouping cells by cluster. Detailed scripts of analysis can be found on the
313 Cotney Lab GitHub (https://github.com/emmawwinchester/mousepalate).

314 *Spatial RNA Sequencing (spRNA-seq, 10x Genomics, Visium).*

315 All steps from 10X Genomics' FFPE Visium Spatial workflow (SpaceRanger) were followed
316 (protocol CG000407 Rev D). Spatial RNA sequencing (spRNA-seq) slides are coated with an
317 array of poly-T primers, which encode unique spatial barcodes. FFPE murine craniofacial tissue
318 from E13.5 and E15.5 embryos was sectioned directly onto the barcoded slide, H&E stained,
319 then underwent enzymatic permeabilization, which allowed for mRNA release and subsequent
320 capture by primer-coated slides. Samples were sequenced on an Illumina NovaSeq6000. All

321 spatial sequencing gene enrichment analyses were conducted using the 10X Genomics Loupe
322 Browser.

323 *Fluorescent Multiplex mRNA In Situ Hybridization (RNAscope).*

324 Mouse embryos were collected in biological triplicates and fixed in 10% formalin for 24 hours.
325 Samples were then processed to paraffin embedding and were sectioned at 5 µm with a Leica
326 RM2255 microtome (Leica Biosystems). RNAscope multiplex fluorescent v2 assay (Advanced
327 Cell Diagnostics, 323100) was used for *in situ* hybridization according to the manufacturer's
328 instructions with modified pretreatment custom reagent for antigen retrieval. RNAscope
329 hybridization has been validated in our laboratory using positive and negative control probes.
330 Marker probes from Advanced Cell Diagnostics were used in this study. Each experiment
331 included a negative control section excluding marker probes for quality control. Representative
332 serial slides were also stained with hematoxylin and eosin (H&E) for histomorphometry context.
333 The fluorescent slides were imaged on an AxioScan.Z1 slide scanner (Zeiss) with Plan-
334 apochromat 40x/0.95 objective in five fluorescent channels (DAPI, FITC, Cy3, Cy5, Cy7). The
335 following gene marker probes were used: RNAscope™ Probe- Mm-Alpl (Cat No. 441161), ,
336 RNAscope™ Probe- Mm-Sost (Cat No. 410031), RNAscope™ Probe- Mm-Six2 (Cat No.
337 500011), RNAscope™ Probe- Mm-Runx2 (Cat No. 414021), RNAscope™ Probe- Mm-Sp7 (Cat
338 No. 403401), RNAscope™ Probe- Mm-Dmp1 (Cat No. 441171), RNAscope™ Probe- Mm-Pax9
339 (Cat No. 454321), RNAscope™ Probe- Mm-Dkk1 (Cat No. 402521), RNAscope™ Probe- Mm-
340 Dkk2 (Cat No. 404841). All slides were counterstained with DAPI (Cat No. 320858)

341 *Modified pentachrome histochemical staining and picrosirius red polarized light imaging.*
342 Modified pentachrome staining was applied to deparaffinized, rehydrated coronal mouse embryo
343 sections from E13.5 and E15.5 in biological triplicate. Rehydrated sections were pretreated with

344 6% nitric acid, then sequentially stained with0.1% toluidine blue (EMS, Cat No. 26074-15) and
345 picrosirius red (Abcam, Cat No. ab246832). Slides were dehydrated and mounted with in
346 toluene-based medium. Stained sections were imaged using an AxioScan.Z1 slide scanner
347 (Zeiss) with Plan-apochromat 40x/0.95 objective in brightfield. Bright-field and dark-field
348 polarized transmission images were acquired via a 10X/0.3NA objective using an Olympus
349 BX51 microscope (Olympus) equipped with a condenser with NA adjusted to 0.3, a rotatable
350 sample stage and Infinity 2C color camera (Luminera). White balance of the camera was
351 adjusted using a bright-field image of a sample slide area near a sample. For dark-field images, a
352 rotatable polarizer and polarizer-analyzer crossed at 90° were introduced into the microscope
353 light path.

354 *Micro-computed tomography (CT) 3D-reconstruction and segmentation.*

355 Embryonic day 15.5 heads fixed overnight in 10% NBF were scanned using a ScanCo µCT 50 *ex*
356 *vivo* cabinet system (Scanco Medical, Brüttisellen, Switzerland) in 70% ethanol using the
357 following parameters: 70kVp, 85µA, 0.5mm AI filter, 900-ms integration time, and 10µm voxel
358 size. 3D rendering and segmentation of reconstructed files were performed using 3D Slicer
359 software (slicer.org) using the semi-automatic segmentation function 'Islands', with standardized
360 thresholding and island size.

361

362

363

364

Acknowledgments. We thank the Microscopy and Imaging Core (NICHD) for their help with the fluorescence imaging; Drs. Sergey Leiken and Elena Makareeva (NICHD) for their technical and analytical support in establishing our independent next-generation sequencing workflow and multiplexed in situ hybridization assays, as well as Dr. Edward Mertz (NICHD) for his assistance in polarized light imaging of picrosirius red stained slides. We are grateful to Dr. Vardit Kram (NIDCR) for her guidance with microCT scanning and analysis. Finally, we want to acknowledge Dr. Ricardo D. Coletta (University of Campinas, FOP, Brazil) for his review and feedback during manuscript preparation.

Funding. National Institutes of Health, National Institute of Dental and Craniofacial Research (RDS); National Institutes of Health, National Institute of Child Health and Human Development, Intramural Research Training Award (JOP/DMR); 1F30DE031149-01, 5R03DE028588-02, 2R35GM119465-06, 5R01DE028945-04 (JLC).

Competing interests. Authors declare that they have no competing interests.

Data and materials availability. All results and analysis data are available in the main text or the supplementary materials. Additional information and materials are available from the corresponding author upon reasonable request.

387 **REFERENCES**

388 BAEK, J. A., LAN, Y., LIU, H., MALTBY, K. M., MISHINA, Y. & JIANG, R. 2011. Bmpr1a
389 signaling plays critical roles in palatal shelf growth and palatal bone formation. *Dev Biol,*
390 350**,** 520-31.
391 BUSH, J. O. & JIANG, R. 2012. Palatogenesis: morphogenetic and molecular mechanisms of
392 secondary palate development. *Development,* 139**,** 231-43.
393 CRUCIAT, C. M. & NIEHRS, C. 2013. Secreted and transmembrane wnt inhibitors and
394 activators. *Cold Spring Harb Perspect Biol,* 5**,** a015081.
395 DINCEL, A. S., JORGENSEN, N. R. & METABOLISM, I.-I. J. C. O. B. 2022. New Emerging
396 Biomarkers for Bone Disease: Sclerostin and Dickkopf-1 (DKK1). *Calcif Tissue Int*.
397 GLASS, D. A., 2ND, BIALEK, P., AHN, J. D., STARBUCK, M., PATEL, M. S., CLEVERS,
398 H., TAKETO, M. M., LONG, F., MCMAHON, A. P., LANG, R. A. & KARSENTY, G.
399 2005. Canonical Wnt signaling in differentiated osteoblasts controls osteoclast
400 differentiation. *Dev Cell,* 8**,** 751-64.
401 HAMACHI, T., SASAKI, Y., HIDAKA, K. & NAKATA, M. 2003. Association between palatal
402 morphogenesis and Pax9 expression pattern in CL/Fr embryos with clefting during
403 palatal development. *Arch Oral Biol,* 48**,** 581-7.
404 HILLIARD, S. A., YU, L., GU, S., ZHANG, Z. & CHEN, Y. P. 2005. Regional regulation of
405 palatal growth and patterning along the anterior-posterior axis in mice. *J Anat,* 207**,** 655-
406 67.
407 HUYBRECHTS, Y., MORTIER, G., BOUDIN, E. & VAN HUL, W. 2020. WNT Signaling and
408 Bone: Lessons From Skeletal Dysplasias and Disorders. *Front Endocrinol (Lausanne),*
409 11**,** 165.
410 ICHIKAWA, E., WATANABE, A., NAKANO, Y., AKITA, S., HIRANO, A., KINOSHITA, A.,
411 KONDO, S., KISHINO, T., UCHIYAMA, T., NIIKAWA, N. & YOSHIURA, K. I. 2006.
412 PAX9 and TGFB3 are linked to susceptibility to nonsyndromic cleft lip with or without
413 cleft palate in the Japanese: population-based and family-based candidate gene analyses.
414 *J Hum Genet,* 51**,** 38-46.
415 JANECKOVA, E., FENG, J., GUO, T., HAN, X., GHOBADI, A., ARAUJO-VILLALBA, A.,
416 RAHMAN, M. S., ZIAEI, H., HO, T. V., PAREEK, S., ALVAREZ, J. & CHAI, Y. 2023.
417 Canonical Wnt signaling regulates soft palate development by mediating ciliary
418 homeostasis. *Development,* 150.
419 JI, Y., GARLAND, M. A., SUN, B., ZHANG, S., REYNOLDS, K., MCMAHON, M.,
420 RAJAKUMAR, R., ISLAM, M. S., LIU, Y., CHEN, Y. & ZHOU, C. J. 2020. Cellular
421 and developmental basis of orofacial clefts. *Birth Defects Res,* 112**,** 1558-1587.
422 JIA, S., ZHOU, J. & D'SOUZA, R. N. 2020. Pax9's dual roles in modulating Wnt signaling
423 during murine palatogenesis. *Dev Dyn,* 249**,** 1274-1284.
424 JIA, S., ZHOU, J., FANELLI, C., WEE, Y., BONDS, J., SCHNEIDER, P., MUES, G. &
425 D'SOUZA, R. N. 2017a. Small-molecule Wnt agonists correct cleft palates in Pax9
426 mutant mice in utero. *Development,* 144**,** 3819-3828.
427 JIA, S., ZHOU, J., WEE, Y., MIKKOLA, M. L., SCHNEIDER, P. & D'SOUZA, R. N. 2017b.
428 Anti-EDAR Agonist Antibody Therapy Resolves Palate Defects in Pax9(-/-) Mice. *J*
429 *Dent Res,* 96**,** 1282-1289.
430 JOENG, K. S., LEE, Y. C., LIM, J., CHEN, Y., JIANG, M. M., MUNIVEZ, E., AMBROSE, C.
431 & LEE, B. H. 2017. Osteocyte-specific WNT1 regulates osteoblast function during bone
432 homeostasis. *J Clin Invest,* 127**,** 2678-2688.

433 KIM, W., KIM, M. & JHO, E. H. 2013. Wnt/beta-catenin signalling: from plasma membrane to
434 nucleus. *Biochem J,* 450**,** 9-21.
435 KRISHNAN, V., BRYANT, H. U. & MACDOUGALD, O. A. 2006. Regulation of bone mass
436 by Wnt signaling. *J Clin Invest,* 116**,** 1202-9.
437 LI, C., LAN, Y. & JIANG, R. 2017a. Molecular and Cellular Mechanisms of Palate
438 Development. *J Dent Res,* 96**,** 1184-1191.
439 LI, C., LAN, Y., KRUMLAUF, R. & JIANG, R. 2017b. Modulating Wnt Signaling Rescues
440 Palate Morphogenesis in Pax9 Mutant Mice. *J Dent Res,* 96**,** 1273-1281.
441 LI, N., LIU, J., LIU, H., WANG, S., HU, P., ZHOU, H., XIAO, J. & LIU, C. 2021. Altered
442 BMP-Smad4 signaling causes complete cleft palate by disturbing osteogenesis in palatal
443 mesenchyme. *J Mol Histol,* 52**,** 45-61.
444 MARTINEZ-GIL, N., UGARTONDO, N., GRINBERG, D. & BALCELLS, S. 2022. Wnt
445 Pathway Extracellular Components and Their Essential Roles in Bone Homeostasis.
446 *Genes (Basel),* 13.
447 MORI-AKIYAMA, Y., AKIYAMA, H., ROWITCH, D. H. & DE CROMBRUGGHE, B. 2003.
448 Sox9 is required for determination of the chondrogenic cell lineage in the cranial neural
449 crest. *Proc Natl Acad Sci U S A,* 100**,** 9360-5.
450 NAGASAKA, A., SAKIYAMA, K., BANDO, Y., YAMAMOTO, M., ABE, S. & AMANO, O.
451 2022. Spatiotemporal Gene Expression Regions along the Anterior-Posterior Axis in
452 Mouse Embryos before and after Palatal Elevation. *Int J Mol Sci,* 23.
453 NEUBUSER, A., PETERS, H., BALLING, R. & MARTIN, G. R. 1997. Antagonistic
454 interactions between FGF and BMP signaling pathways: a mechanism for positioning the
455 sites of tooth formation. *Cell,* 90**,** 247-55.
456 OLIVER, J. D., JIA, S., HALPERN, L. R., GRAHAM, E. M., TURNER, E. C., COLOMBO, J.
457 S., GRAINGER, D. W. & D'SOUZA, R. N. 2021. Innovative Molecular and Cellular
458 Therapeutics in Cleft Palate Tissue Engineering. *Tissue Eng Part B Rev,* 27**,** 215-237.
459 OLIVER, J. D., TURNER, E. C., HALPERN, L. R., JIA, S., SCHNEIDER, P. & D'SOUZA, R.
460 N. 2020. Molecular Diagnostics and In Utero Therapeutics for Orofacial Clefts. *J Dent*
461 *Res,* 99**,** 1221-1227.
462 PAUDEL, S., GJORCHESKA, S., BUMP, P. & BARSKE, L. 2022. Patterning of cartilaginous
463 condensations in the developing facial skeleton. *Dev Biol,* 486**,** 44-55.
464 PETERS, H., NEUBUSER, A., KRATOCHWIL, K. & BALLING, R. 1998. Pax9-deficient mice
465 lack pharyngeal pouch derivatives and teeth and exhibit craniofacial and limb
466 abnormalities. *Genes Dev,* 12**,** 2735-47.
467 PETERS, H., WILM, B., SAKAI, N., IMAI, K., MAAS, R. & BALLING, R. 1999. Pax1 and
468 Pax9 synergistically regulate vertebral column development. *Development,* 126**,** 5399-
469 408.
470 PIÑA, J. O., RAJU, R., ROTH, D. M., CHATTARAJ, P., KIDWAI, F., FAUCZ, F. R., IBEN, J.,
471 MITRA, A., CAMPBELL, K., FRIDELL, G., ESNAULT, C., DALE, R. K. &
472 D'SOUZA, R. N. 2023. Integrated spatiotemporal transcriptomic resolution of embryonic
473 palate osteogenesis. *bioRxiv***,** 2023.03.30.534875.
474 REGARD, J. B., CHERMAN, N., PALMER, D., KUZNETSOV, S. A., CELI, F. S.,
475 GUETTIER, J. M., CHEN, M., BHATTACHARYYA, N., WESS, J., COUGHLIN, S.
476 R., WEINSTEIN, L. S., COLLINS, M. T., ROBEY, P. G. & YANG, Y. 2011. Wnt/beta-
477 catenin signaling is differentially regulated by Galpha proteins and contributes to fibrous
478 dysplasia. *Proc Natl Acad Sci U S A,* 108**,** 20101-6.

REYNOLDS, K., KUMARI, P., SEPULVEDA RINCON, L., GU, R., JI, Y., KUMAR, S. & ZHOU, C. J. 2019. Wnt signaling in orofacial clefts: crosstalk, pathogenesis and models. *Dis Model Mech,* 12.

SASAKI, Y., O'KANE, S., DIXON, J., DIXON, M. J. & FERGUSON, M. W. 2007. Temporal and spatial expression of Pax9 and Sonic hedgehog during development of normal mouse palates and cleft palates in TGF-beta3 null embryos. *Arch Oral Biol,* 52**,** 260-7.

SHAFFER, J. R., ORLOVA, E., LEE, M. K., LESLIE, E. J., RAFFENSPERGER, Z. D., HEIKE, C. L., CUNNINGHAM, M. L., HECHT, J. T., KAU, C. H., NIDEY, N. L., MORENO, L. M., WEHBY, G. L., MURRAY, J. C., LAURIE, C. A., LAURIE, C. C., COLE, J., FERRARA, T., SANTORICO, S., KLEIN, O., MIO, W., FEINGOLD, E., HALLGRIMSSON, B., SPRITZ, R. A., MARAZITA, M. L. & WEINBERG, S. M. 2016. Genome-Wide Association Study Reveals Multiple Loci Influencing Normal Human Facial Morphology. *PLoS Genet,* 12**,** e1006149.

SWEAT, Y. Y., SWEAT, M., MANSARAY, M., CAO, H., ELIASON, S., ADEYEMO, W. L., GOWANS, L. J. J., ESHETE, M. A., ANAND, D., CHALKLEY, C., SAADI, I., LACHKE, S. A., BUTALI, A. & AMENDT, B. A. 2020. Six2 regulates Pax9 expression, palatogenesis and craniofacial bone formation. *Dev Biol,* 458**,** 246-256.

WANG, L., TANG, Q., XU, J., LI, H., YANG, T., LI, L., MACHON, O., HU, T. & CHEN, Y. 2020. The transcriptional regulator MEIS2 sets up the ground state for palatal osteogenesis in mice. *J Biol Chem,* 295**,** 5449-5460.

ZHOU, J., GAO, Y., LAN, Y., JIA, S. & JIANG, R. 2013. Pax9 regulates a molecular network involving Bmp4, Fgf10, Shh signaling and the Osr2 transcription factor to control palate morphogenesis. *Development,* 140**,** 4709-18.

517 **FIGURE LEGENDS**

518 **Figure 1. A gradient of *Pax9* expression guides expansion of ossification centers in the**
519 **developing palate.** A) Hematoxylin and eosin (H&E) stained palatal shelves (ps) at embryonic
520 days 13.5 and E15.5 orienting toward relevant anatomy within the surrounding region. Notably,
521 in normal development, mineralized bone is not seen in the palatal shelf mesenchyme at
522 embryonic day 13.5, while it is present by E15.5. Asterisk (*) indicates mesenchymal
523 condensation prior to bone formation. B) Whole-transcriptome spatially resolved RNA-
524 sequencing (*Visium, 10x Genomics*) of the posterior secondary palate at E13.5 and E15.5
525 visualizing enriched *Pax9, Sp7,* and *Cd200* gene expression. Orange to red color scale represents
526 increasing $\log_2$-fold gene enrichment. B') Globally distinguishing significant feature comparison
527 between manually selected osteogenic and mesenchymal barcode clusters at E15.5. Panels,
528 clockwise, represent log2-fold gene enrichment of *Pax9*, progenitor cell markers (*Six2, Erg,*
529 *Crabp1*), osteoblast markers (*Cd200, Bglap, Ifitm5*), and osteocytes (*Sost, Dmp1, Phex)*. C)
530 Single-nucleus gene and epigenetic sequencing (*Multiome RNA+ATAC-seq, 10x Genomics, Inc.*)
531 of the murine embryonic secondary palate. C') Annotated cell populations present in the E13.5
532 and E15.5 secondary palate include canonical cell types, with the addition of *Pax9*+
533 Mesenchyme. C'') Enrichment of *Pax9* expression in *Pax9*+ Mesenchyme compared to all other
534 cell types in the secondary palate. C''') Bias of *Pax9* binding motif in regions of chromatin
535 uniquely accessible in *Pax9*+ Mesenchyme.

536

537 **Figure 2. Evidence of *Pax9*$^{-/-}$ palatal bone premature formation.** A) Modified pentachrome
538 staining of E13.5 and E15.5 palatal shelves demonstrating distribution of collagen fibrils in red
539 (A, B) and their organization under polarized light, ranging from orange to green color

540 depending on degree of birefringence (A', B'). pb: palatine bone; nc: nasal cavity; m: molar. C)
541 Hematoxylin & eosin stain and multiplexed mRNA *in situ* hybridization (RNAscope) on
542 adjacent serial sections highlighting hallmark features of bone maturation within the palatal bone
543 ossification zone of *Pax9*$^{+/+}$ and *Pax9*$^{-/-}$ mice. Black arrows indicate trabeculae within palatine
544 bone. Merged images represent *Sost*+ osteocytes (red) in the context of osteogenic *Alpl* (yellow),
545 with blue DAPI+ nuclei. White dotted overlay corresponds to borders of bone. D) Micro-
546 computed tomography 3D reconstruction of paired maxillary (yellow) and palatine bones
547 (blue)(D'), presented from a superior axial view (top) and coronal orthogonal slice (bottom) of
548 similar depth to histological sections. Dotted outline represents control bone silhouette
549 superimposed over knockout bone.
550
551 **Figure 3. Loss of *Pax9* alters patterning of the palate osteodifferentiation gradient.**
552 RNAscope *in situ* hybridization targeting osteogenic populations using probes for *Six2, Runx2,*
553 *Dmp1,* and *Dkk2.* A) Co-staining of progenitors (*Six2*, green), pre-osteoblasts (*Runx2*, red), and
554 immature osteocytes (*Dmp1,* white) in coronal control (*Pax9*$^{+/+}$) and knockout (*Pax9*$^{-/-}$) palatal
555 shelves at E13.5. Blue (A') and red (A") cropped regions highlight osteodifferentiation gradients.
556 Green, red, and yellow arrowheads indicate examples of *Six2*+ cells, *Runx2*+ cells, and
557 *Six2+/Runx2*+ cells (respectively). od: oral domain; nd: nasal domain B) Co-staining of pre-
558 osteoblasts (*Runx2*, red), osteoblasts (*Sp7*, yellow), and immature osteocytes (*Dmp1*, magenta)
559 with Wnt signaling modulator *Dkk2* (green) at E15.5. Blue (B') and red (B") cropped regions
560 focus on osteogenic fronts in the Pax9$^{+/+}$ and Pax9$^{-/-}$ palate. Colored bars in B'' represent range
561 of expression domains observed for each mRNA target, according to the color scheme in B.
562 Overlapping colored bars indicate co-expression. Green arrows highlight limited *Dkk2*

563 expression in Pax9$^{+/+}$ embryos. C', C") High magnification image at terminal boundary of
564 osteogenic front, highlighting relative distribution and spacing of *Runx2* (red), *Sp7* (green), and
565 *Dmp1* (white) expressing cells.
566
567 **Figure 4. *Dkk2*, in concert with *Pax9*, coordinates zones of osteogenic differentiation in the**
568 **developing palate.**
569 A) RNAscope *in situ* hybridization targeting *Pax9* (green), Wnt modulators *Dkk1* (red) and *Dkk2*
570 (magenta), and osteogenic *Alpl* (yellow) at embryonic day 13.5 (E13.5). White dotted lines
571 outline margins of palatal shelf. Asterisk (*) indicates osteogenic center in Pax9$^{-/-}$ mice. B)
572 Cropped regions of interest from experiment pictured in (A) from ossification center (top) and
573 mesial edge of palate nasal domain (bottom). Merged ossification center region of interest is split
574 into individual stains along arrows (green *Pax9,* magenta *Dkk2*, yellow *Alpl*). C) Schematic
575 summary of the shifting landscape of Wnt-regulated osteogenesis in the E13.5 embryonic palate
576 with the loss of *Pax9*.
577

Fig. 1

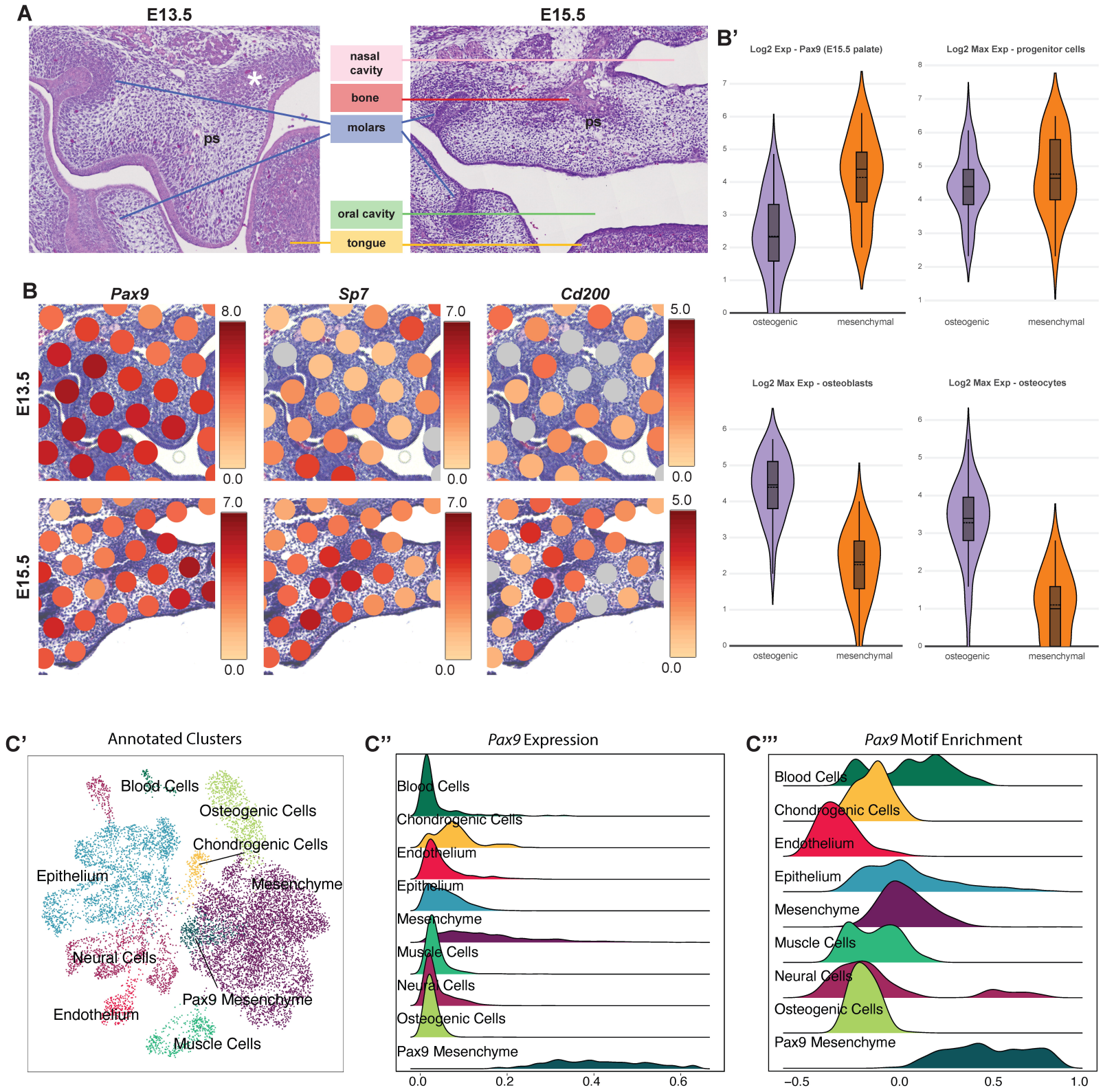
A
E13.5
E15.5
nasal cavity
bone
molars
oral cavity
tongue
ps
ps
B
Pax9
Sp7
Cd200
E13.5
E15.5
8.0
7.0
5.0
0.0
B'
Log2 Exp - Pax9 (E15.5 palate)
Log2 Max Exp - progenitor cells
Log2 Max Exp - osteoblasts
Log2 Max Exp - osteocytes
osteogenic
mesenchymal
C'
Annotated Clusters
Blood Cells
Osteogenic Cells
Chondrogenic Cells
Epithelium
Mesenchyme
Neural Cells
Pax9 Mesenchyme
Endothelium
Muscle Cells
C''
Pax9 Expression
Blood Cells
Chondrogenic Cells
Endothelium
Epithelium
Mesenchyme
Muscle Cells
Neural Cells
Osteogenic Cells
Pax9 Mesenchyme
0.0
0.2
0.4
0.6
C'''
Pax9 Motif Enrichment
Blood Cells
Chondrogenic Cells
Endothelium
Epithelium
Mesenchyme
Muscle Cells
Neural Cells
Osteogenic Cells
Pax9 Mesenchyme
−0.5
0.0
0.5
1.0

Fig. 2

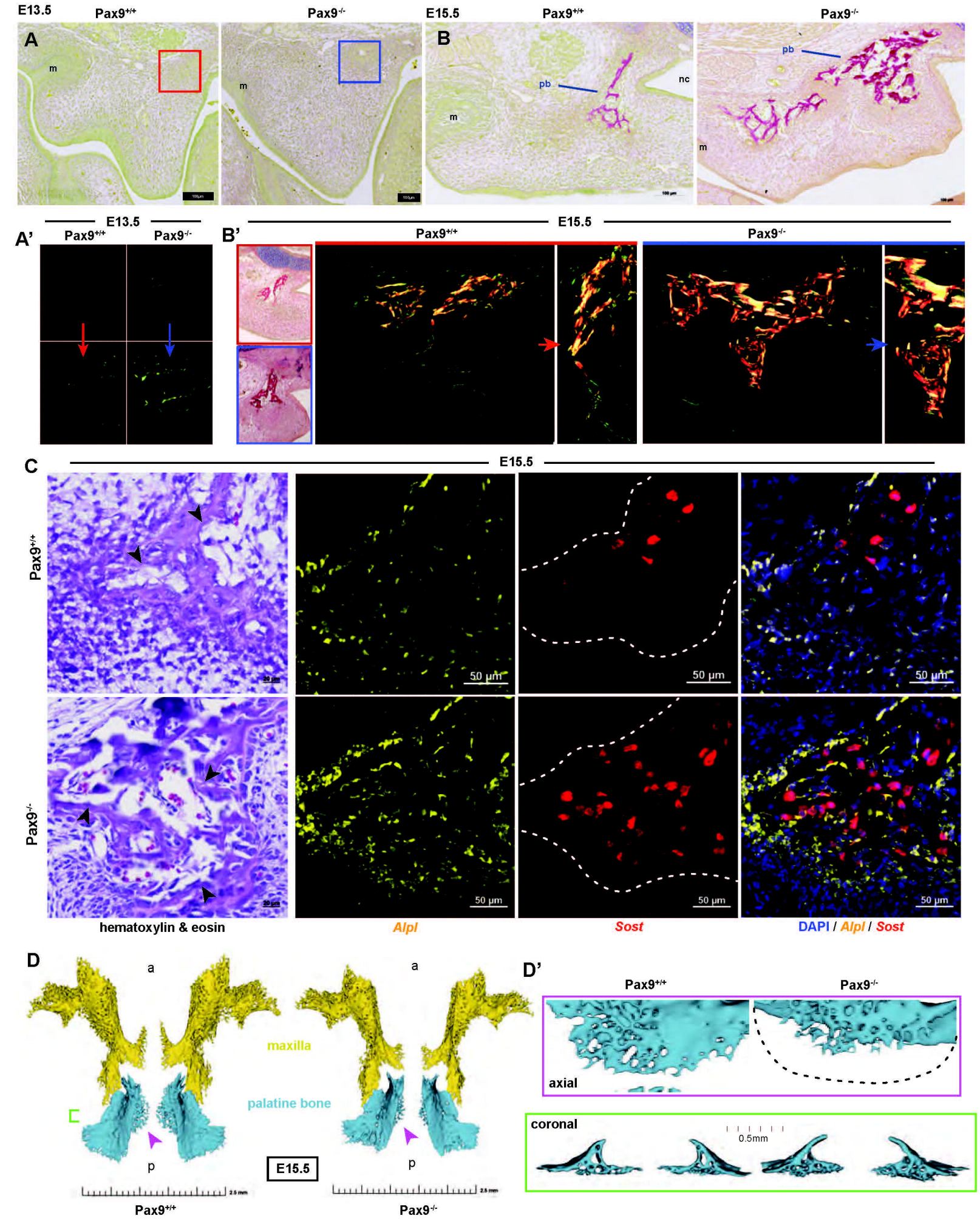
E13.5
Pax9+/+
Pax9-/-
E15.5
Pax9+/+
Pax9-/-
A
B
m
pb
nc
A'
B'
C
Pax9+/+
Pax9-/-
50 µm
hematoxylin & eosin
Alpl
Sost
DAPI / Alpl / Sost
D
D'
a
p
maxilla
palatine bone
E15.5
axial
coronal
0.5mm

Fig. 3

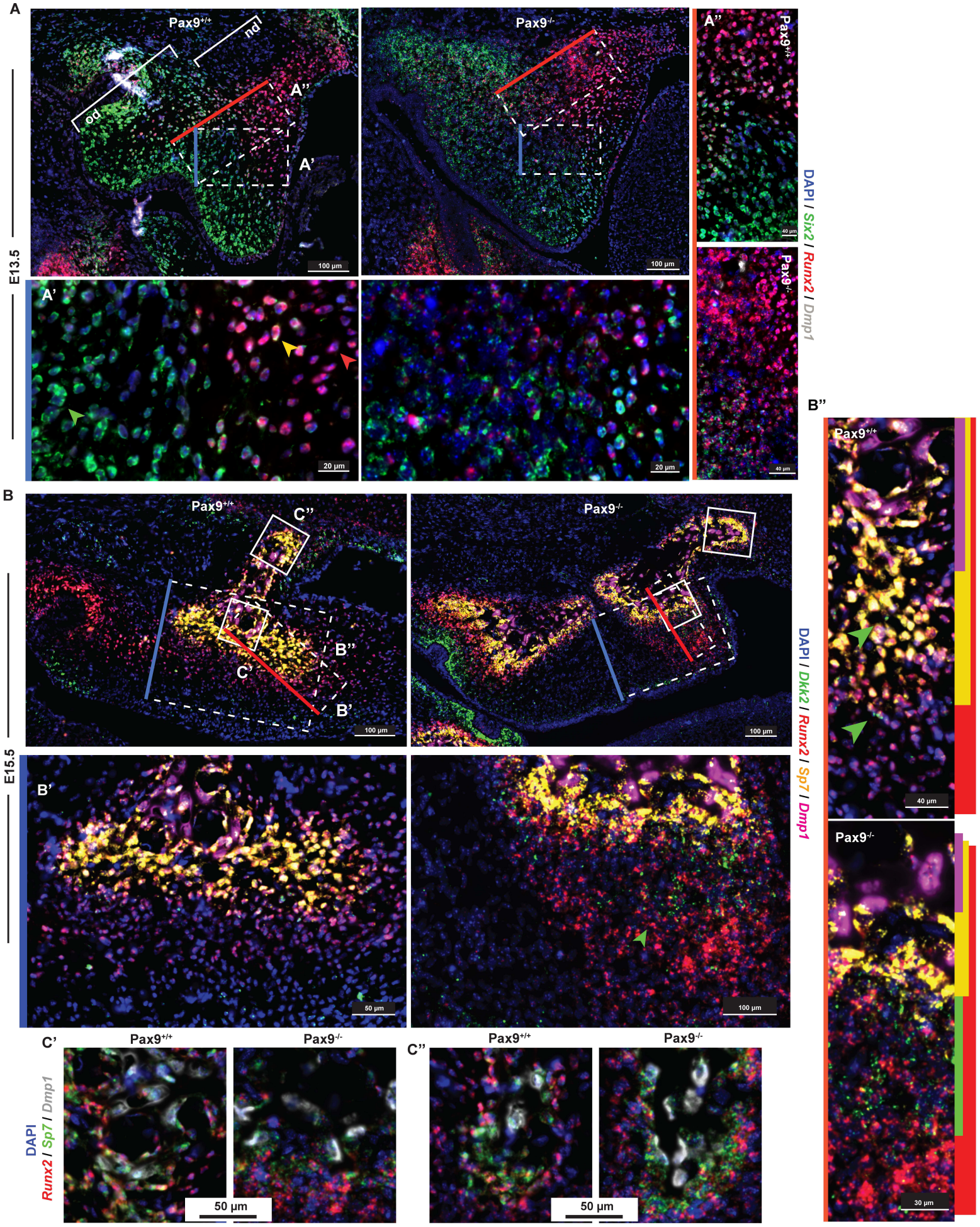

A
Pax9+/+
nd
od
A''
A'
Pax9-/-
100 µm
20 µm
40 µm
E13.5
DAPI / Six2 / Runx2 / Dmp1
B
C''
B''
C'
B'
E15.5
DAPI / Dkk2 / Runx2 / Sp7 / Dmp1
50 µm
30 µm
C'
C''
DAPI
Runx2 / Sp7 / Dmp1

Fig. 4

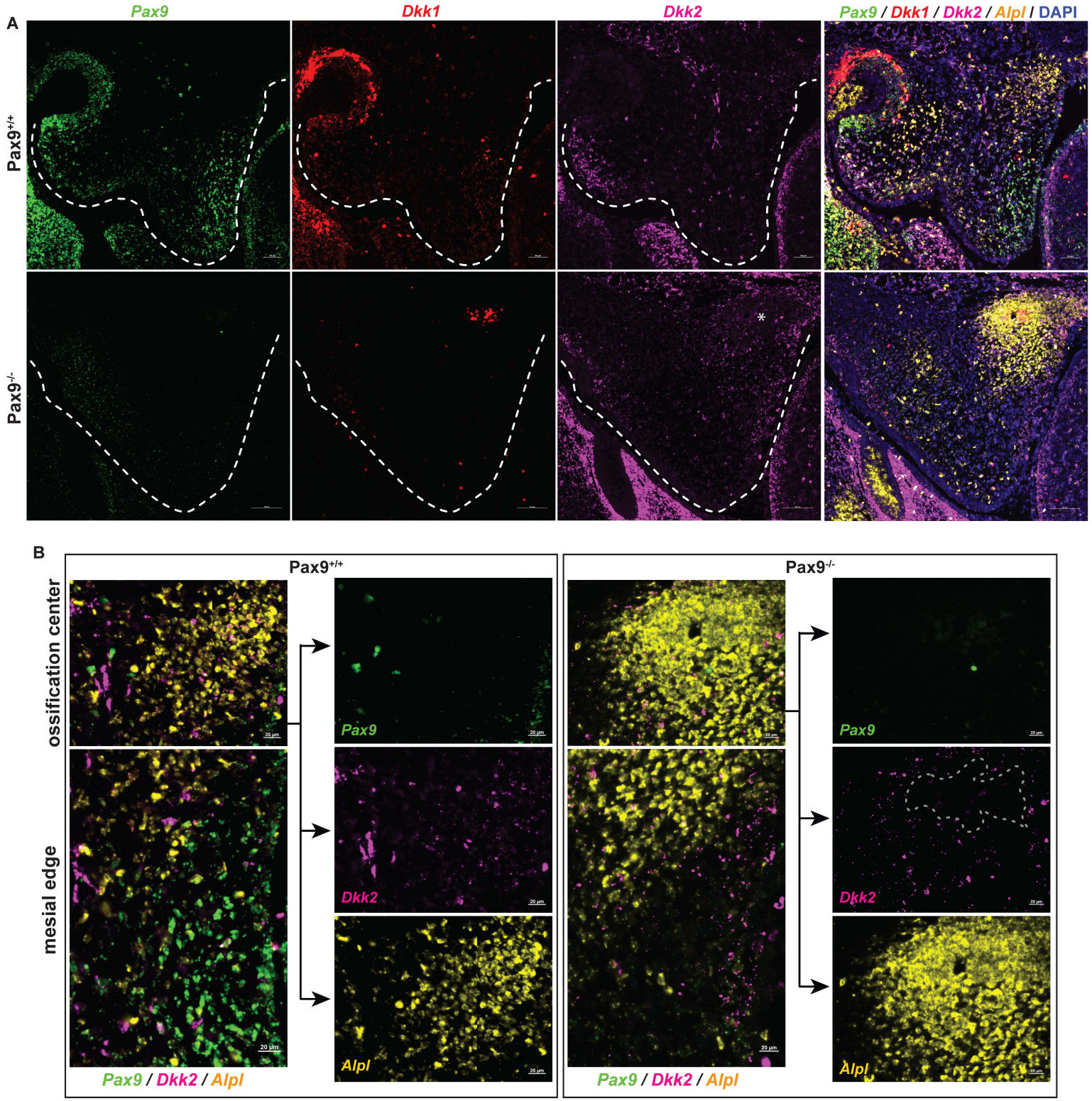
A
Pax9
Dkk1
Dkk2
Pax9 / Dkk1 / Dkk2 / Alpl / DAPI
Pax9+/+
Pax9-/-
*
B
Pax9+/+
Pax9-/-
ossification center
mesial edge
Pax9
Dkk2
Alpl
Pax9 / Dkk2 / Alpl
20 µm

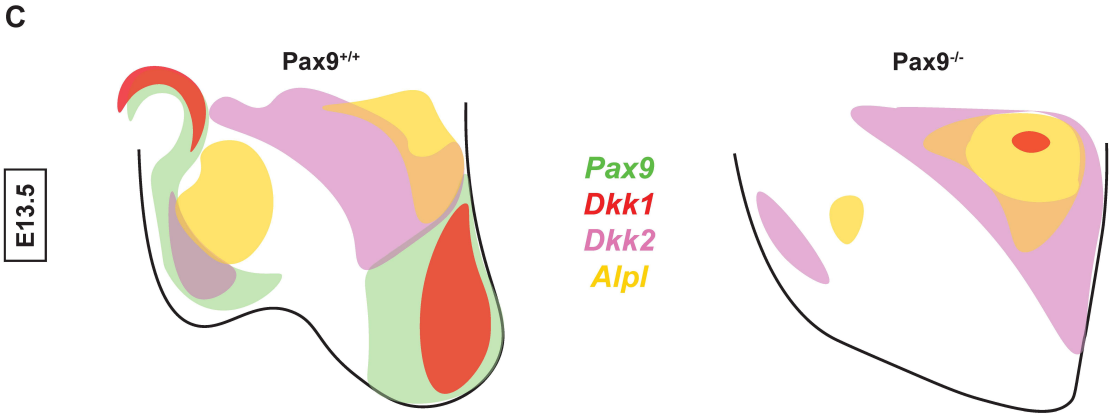
C
E13.5
Pax9+/+
Pax9-/-
Pax9
Dkk1
Dkk2
Alpl